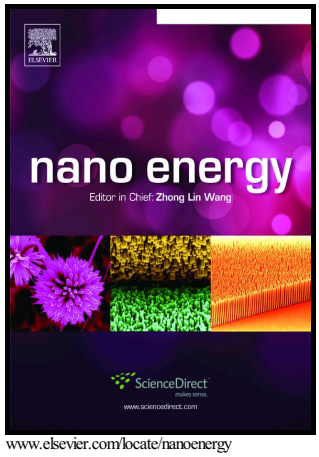

www.elsevier.com/locate/nanoenergy

Biomass Derived Carbon Nanoparticle as anodes for High Performance Sodium and Lithium Ion Batteries

Rohit Ranganathan Gaddam, Dongfang Yang, Ramanuj Narayan, KVSN Raju, Nanjundan Ashok Kumar, X.S. Zhao

PII: S2211-2855(16)30171-9
DOI: http://dx.doi.org/10.1016/j.nanoen.2016.05.047
Reference: NANOEN1312

To appear in: *Nano Energy*

Received date: 21 March 2016
Revised date: 20 May 2016
Accepted date: 26 May 2016

Cite this article as: Rohit Ranganathan Gaddam, Dongfang Yang, Ramanuj Narayan, KVSN Raju, Nanjundan Ashok Kumar and X.S. Zhao, Biomass Derived Carbon Nanoparticle as anodes for High Performance Sodium and Lithium Ion Batteries, *Nano Energy* http://dx.doi.org/10.1016/j.nanoen.2016.05.047

Biomass Derived Carbon Nanoparticle as anodes for High Performance Sodium and Lithium Ion Batteries

Rohit Ranganathan Gaddam[a], Dongfang Yang[a], Ramanuj Narayan[b], KVSN Raju[b], Nanjundan Ashok Kumar[a,*], X.S. Zhao[a,*]

[a]*School of Chemical Engineering, The University of Queensland, St Lucia, Brisbane 4072 Australia.*

[b]*Polymers and Functional Materials Division, CSIR-Indian Institute of Chemical Technology, Hyderabad 500007, India.*

george.zhao@uq.edu.au

ashok.nanjundan@uq.edu.au

[*]Corresponding authors:

Abstract

In this paper, we report a flame deposition method to prepare carbon nanoparticles (CNPs) from coconut oil. The CNPs were further modified with a piranha solution to obtain surface-carboxylated carbon nanoparticles (*c*-CNPs). When used as an anode for sodium-ion batteries, the CNPs and *c*-CNPs respectively delivered discharge capacities of 277 and 278 $mAhg^{-1}$ in the second cycle at a current density of 100 mAg^{-1}. At the 20^{th} cycle, the capacities of CNP and c-CNPs were 217 and 206 $mAhg^{-1}$ respectively. The results suggest that modification of the CNPs with the piranha solution improved neither the charge storage capacity nor the stability against cycling in a sodium-ion battery. When the CNP and *c*-CNP were used an anode in a lithium-ion battery, 2^{nd}-cycle discharge capacities of 741 and 742 $mAhg^{-1}$ respectively at a current density of 100 mAg^{-1} were obtained. After 20 cycles the capacities of CNP and *c*-CNP became 464 and 577 $mAhg^{-1}$ respectively, showing the cycling stability of the CNPs was improved after modification. The excellent cycling performance,

high capacity and good rate capability make the present material as highly promising anodes for both sodium-ion and lithium-ion batteries.

Graphical abstract:

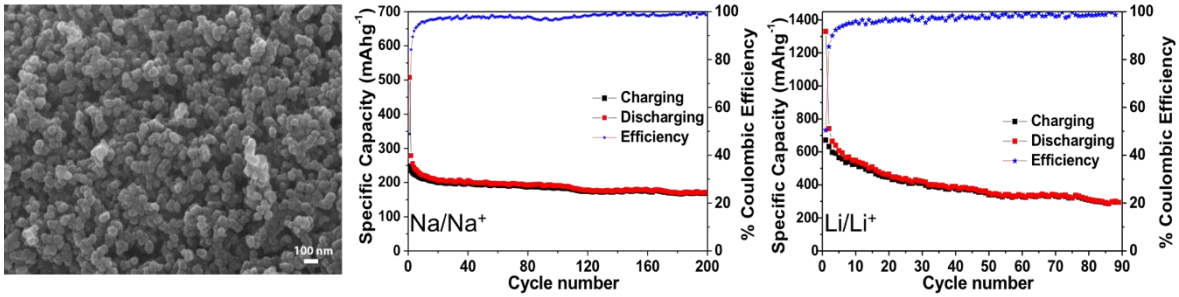

Carbon nanoparticles derived from biomass and their electrochemical performance as anode in both sodium-ion and lithium-ion batteries.

Keywords: bio-mass carbon, anode, battery, sodium-ion, lithium-ion

1. Introduction

Lithium-ion batteries (LIBs) with graphite as the anode are nowadays popularly used to power portable electronic devices. However, the limited theoretical capacity of graphite (372 $mAhg^{-1}$) [1, 2] hinders further development of new-generation LIBs for large-scale energy storage applications. On the other hand, lithium is geographically limited and politically sensitive. Increasing the utilization of lithium in energy storage will definitely increase the cost of LIBs in future [3]. Unlike lithium, sodium is naturally abundant. Sodium-ion batteries (NIBs) are promising alternative for LIBs. However, the graphite anode that is being used in LIBs fails to perform well in a NIB owing to the larger ionic radius of Na (0.102 nm) than that of Li (0.076 nm) and the thermodynamic instability of sodium-graphite system [4]. Therefore, an alternative anode with high performance and low cost is of paramount importance in the development of the NIB technology.

Electrode materials such as transition metal oxides [5-9], graphene [10], metal nitrides [11] and carbons [12-15] have been studied as anodes for NIBs. Carbon materials, especially hard carbon [16], have been shown to be the most promising anode for both NIBs and LIBs [17]. Production of carbon materials from biomass is highly attractive [18]. For battery applications, biomass-derived carbons can usually offer a higher capacity than graphite because biomass intrinsically has desirable molecular structures and architectures, which are favorable for charge storage and transport [19]. Since the raw material is naturally available no tedious approaches need to be realized for material engineering, which itself is an economic solution [19].

Herein, we present a flame deposition method to synthesize carbon nanoparticles (CNPs) with coconut oil as the biomass precursor. The coconut oil derived CNPs possessed graphitic domains and displayed a quasi-spherical morphology. The obtained CNPs were further treated with an oxidizing agent to modify the surface of the CNPs to be rich in carboxylic groups [20, 21]. The carbon samples were then tested as anode materials in both LIBs and NIBs. Tested against sodium, the CNPs and *c*-CNPs delivered a capacity of 277 and 278 $mAhg^{-1}$ at a current density of 100 mAg^{-1} in the second cycle. For LIBs, the discharge capacities of CNP and *c*-CNP were 741 and 742 $mAhg^{-1}$ respectively at a current density of 100 mAg^{-1} in the second cycle. The present work has the following advantages: (i) the precursor is cheap and widely available, (ii) the synthesis method is scalable, and (iii) the obtained carbons are dense and show good performance in both NIBs and LIBs.

2. Experimental Section

2.1 Material Preparation

100 g of coconut oil purchased from the local market was taken in a crucible with a cotton wick placed inside. The wick was lit to let incineration of coconut oil imbibed by capillary action. The crucible was then covered with a brass lid with holes to allow air circulation. The carbon nanoparticles (CNPs) in the form of soot deposited on the brass plate was collected. The CNPs were further carboxylated by refluxing in a piranha solution (caution: a highly exothermic mixture of H_2SO_4 and H_2O_2 in the ratio of 7:3) for 6 h and subsequently washed with copious amounts of ethanol and water, filtered and dried in a vacuum oven at 80 °C for 24 h to obtain *c*-CNPs.

2.2 Material Characterization

X-Ray diffraction (XRD) was recorded on Bruker D8 Advance X-ray diffractometer with Ni-filtered Cu Kα radiation (λ = 1.54056 Å; 40 kV, 30 mA) at a scan rate of 2° min^{-1}. Nitrogen sorption isotherms were measured on a Tristar II 3020. All samples were degassed at 150 °C for 3 h prior to the measurement. Transmission electron microscopy (TEM) measurements were carried out on a JEOL 2100 at an acceleration voltage of 200 kV. Field emission scanning electron microscope measurements were taken on JEOL 7001. X-ray photoelectron spectroscopy (XPS) spectra were acquired on a Kratos Axis ULTRA X-ray photoelectron spectrometer with a 165 mm hemispherical electron energy analyzer and a monochromatic Al Kα (1486.6 eV) radiation at 225 W (15 kV, 15 mA). Raman spectra were collected using a Raman Spectrometer (Renishaw) with a 514 nm laser. Thermogravimetric analysis (TGA) was conducted on a Shimadzu simultaneous TGA/DTA analyzer DTG-60 at a heating rate of 10 °C min^{-1} in air of flow rate of 100 mL min^{-1}.

2.3 **Electrochemical Testing**

Typically, a slurry of 70% active material, 20% carbon black and 10 % polyvinyldine fluoride (PVDF) in *N*-methyl pyrrolidine (NMP) was coated onto a copper foil current

collector (~1.5 mg of active material on each electrode) and then dried at 60 °C overnight in a vacuum oven. The obtained electrode, polypropylene separator (for Li), glass fiber (for Na), and Na/Li metal counter electrode were assembled into a 2032-type coin cell filled with an electrolyte in an Ar-filled glovebox with sub-0.1 ppm water and oxygen contents. For the LIB cells, 1 M $LiPF_6$ in ethylene carbonate (EC) and dimethyl carbonate (DC) (1:1) was used as the electrolyte. For the NIB cells, 1 M $NaClO_4$ in equal volume ratio of ethylene carbonate (EC) and propylene carbonate (PC) mixed with 0.3 wt% of fluoroethylene carbonate (FEC) was used. Cyclic voltammetry was carried out using a CHI-600D electrochemical workstation at a scan rate of 0.1 mVs^{-1} in the voltage domain of 0.005 to 3 V. The charge/discharge measurements were performed using a Neware battery tester CT3008. Electrochemical impedance spectroscopy measurements were also performed using a CHI 660D electrochemical workstation in the frequency range of 100 kHz to 10 mHz.

3. Results and Discussion

Figs. 1a and 1b show the FESEM and TEM images of CNPs with a quasi-spherical morphology and particle size ranging from 40 to 50 nm. The CNPs upon treatment with piranha solution show no obvious changes in morphology (Figs. 1c and 1d). Pores within the particles are not obvious from the FESEM and TEM images.

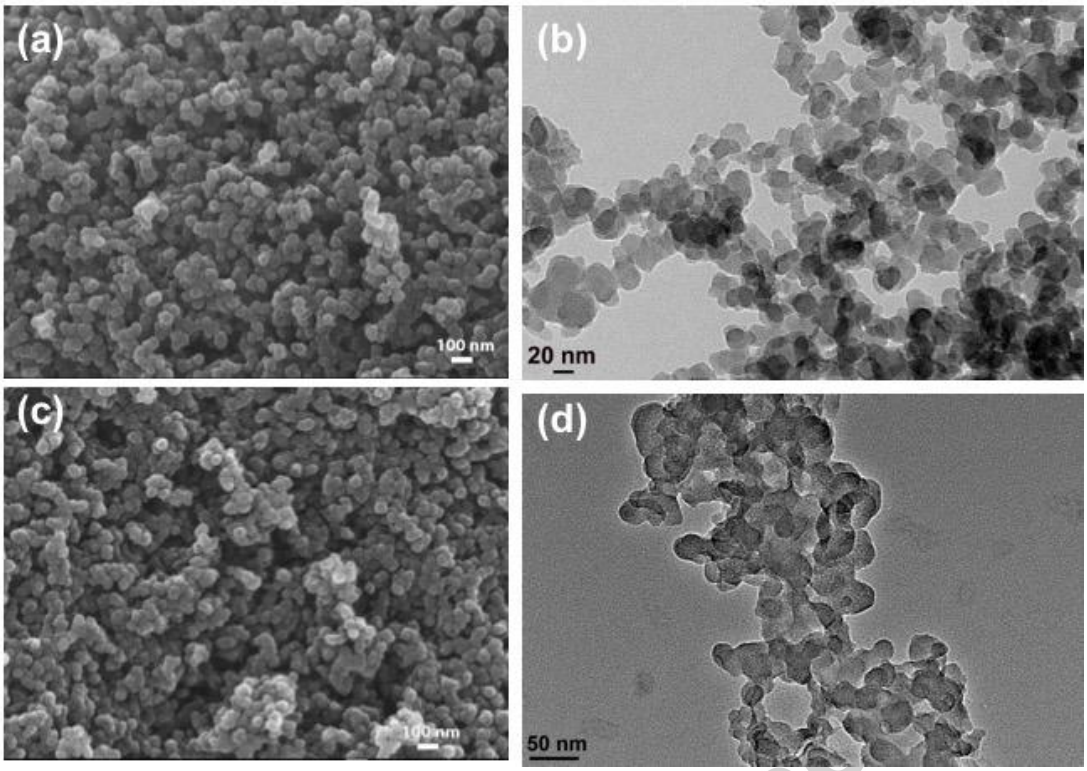

Fig. 1 FESEM and TEM images of pristine carbon nanoparticles (CNPs) (a, c) and (b, d) carboxyl terminated carbon nanoparticle (*c*-CNPs).

The XRD patterns for CNPs and *c*-CNPs show two peaks at about 25° and 45° two theta, which correspond to (002) and (100) reflections of graphite, respectively (Fig. 2a) [22]. An increase in crystallinity of *c*-CNP is evident from the XRD profile. This may be attributed to the nascent oxygen (originating from piranha solution), which generates a cascading effect, favoring the disentanglement of carbon bonds and formation of oxygen sites for carboxyl bond establishment along with the removal of some amorphous carbons [23].

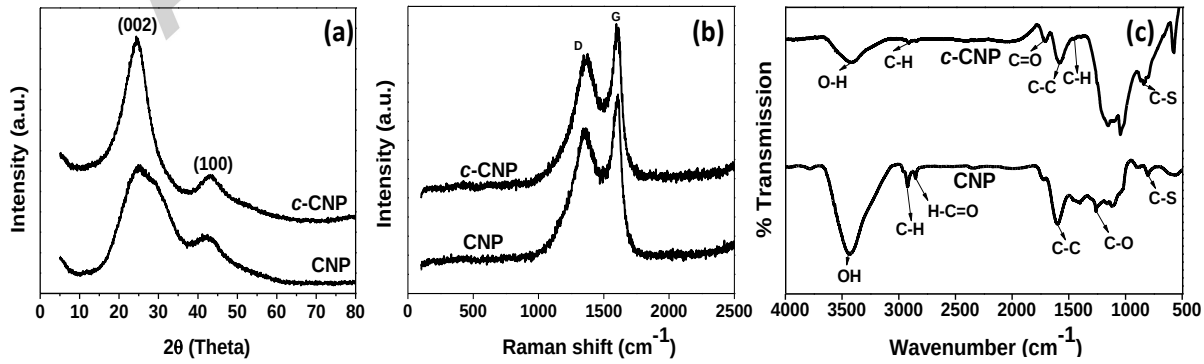

Fig. 2 (a) X-ray diffraction profile (b) Raman spectroscopy (c) FTIR analysis of CNP and c-CNP.

The Raman spectra (Fig. 2b) revealed two significant bands at around 1360 cm^{-1} and 1590 cm^{-1}, corresponding to the D-band and G-band of graphitic carbon, respectively. The D-band represents A_{1g} symmetry of disordered graphite, indicating the existence of crystalline domains in the samples [24, 25]. The G-band corresponds to the zone center symmetry of single crystalline graphite. The intensity ratio of D and G bands also can be used to determine the rate of disorder in the carbon. The I_D/I_G ratios of the samples were calculated to be around 0.854 for CNPs and 0.840 in the case of *c*-CNPs. No distinct differences were observed in the I_D/I_G ratios probably because piranha solution would dissolve active defect sites in the carbons without creating additional defects as observed previously [26]. The superimposition of different Raman modes as a result of the distribution cluster of nanoparticle with different sizes, result in a broader width in case of the CNPs, different from that of the *c*-CNP [27].

The Fourier-transform infrared (FTIR) spectra shown in Fig. 2c exhibited a peak at 1726 cm^{-1} for *c*-CNP, which is due to the C=O stretching [28], confirming the presence of carboxyl groups. This peak could not be observed in CNP. Also an additional peak at 1052 cm^{-1} corresponding to stretching frequency of primary alcohols is observable from *c*-CNP. Both CNP and *c*-CNP contain absorption peaks around 3430 cm^{-1} pertaining to –OH stretching, 2920 cm^{-1} of –C-H- bond and 820 cm^{-1} of -C-S- bond. The C-S bond could possibly arise from ν C-S stretching [23]. The coconut oil contained Sulphur, which gave rise to the C-S bond formation in both CNP and *c*-CNP samples.

The nitrogen adsorption/desorption isotherms and the corresponding pore size distribution curves computed using the Barrett–Joyner–Halenda (BJH) method [29] for both CNP and *c*-CNP are shown in Fig. S2. The obtained isotherms show existence of both micropores and mesopores (type IV). An upward tendency at the high relative pressure

region, P/P_o~0.9-1, can be attributed to the macropores formed between carbon particles [30]. Though the above statement holds true for the as prepared carbon materials, *c*-CNP showed a positive shift from that of CNP showcasing the significant existence of micropores and mesopores (Fig. S1). The surface area of *c*-CNP (133 m^2/g) is higher than that of the CNP (56 m^2/g), indicating the creation of pores during the oxidative treatment using piranha solution. The X–ray Photoelectron spectroscopy (XPS) results for CNP and *c*-CNP samples revealed atomic concentrations of carbon of 93.02 and 80.49 atm.%, oxygen 6.64 and 17.06 atm.%, and sulfur 0.34 and 2.45 atm.%, respectively (Fig. S3). The surface oxygen content upon piranha solution treatment was increased largely. Since the carbons have low surface area, it is not anticipated that oxygen and sulfur functionalities will have a substantial impact on the electrochemical performance [17, 31].

3.1 Electrochemical performance as a sodium-ion battery anode

Sodium-ion storage behavior in CNP and *c*-CNP was evaluated using cyclic voltammetry (CV) and galvanostaic charge-discharge (GCD) techniques. Fig. S4 shows the CV curves of CNP and c-CNP vs Na/Na^+ in the range of 0.005 to 3 V at a sweep rate of 0.1 mVs^{-1}. The CV curves reveal a strong cathodic peak at around 1.0 V in both CNP and *c*-CNP corresponding to the electrolyte decomposition, leading to the formation of solid electrolyte interphase (SEI) on the surface of the electrode [32, 33]. This peak disappeared in the subsequent cycles, indicating the formation of the SEI occurred only in the initial discharge. A redox peak near 0 V similar to that observed during lithium insertion [2], endorse the sodium insertion and de-insertion in the interlayer of the graphitic domains present in the as prepared carbons. The shape of the CV curve being nearly rectangular in nature in the whole voltage range is indicative of the capacitive storage behavior of sodium ions [34]. It may be inferred that sodium-ion interaction with the anode material predominantly takes place by physical interaction, along with some redox reactions due to the interaction between sodium ions and

oxygen containing functional groups during the charge-discharge process [35]. Notably the CV curves overlapped after the initial cycle, indicating the reversible interaction of sodium-ion with the as prepared carbons.

Fig. 3 shows the GCD curves of CNP and *c*-CNPs. An initial discharge capacity of 507 and 733 $mAhg^{-1}$ for CNP and *c*-CNPs respectively was obtained at a current density of 100 $mAhg^{-1}$ with a coulombic efficiency of 49 and 34% (Fig. 3b and 3e). Such large capacity loss and low initial coulombic efficiency is generally observed in carbon materials due to the decomposition of electrolytes on the surface of active site [33], formation of SEI on the electrode surface, side reactions on the electrode surface and trapping of sodium-ions in the voids between the carbon particles [34]. The coulombic efficiency improves to about 88% in the second cycle and stabilizes at more than 96% in the tenth cycle owing to the structural stability of the as prepared carbon materials upon cycling. These observations corroborate with that of CV curves. At the 2^{nd} cycle, the CNP and *c*-CNP show a specific capacity of 278 and 277 $mAhg^{-1}$ respectively. Upon repeated cycling, the coulombic efficiency is increased to near 100% and a capacity of 198 and 203 $mAhg^{-1}$ can still be retained at the 50^{th} cycle (Table S1). The discharge capacity of both samples outperformed most of the carbon materials previously reported (Table 1).

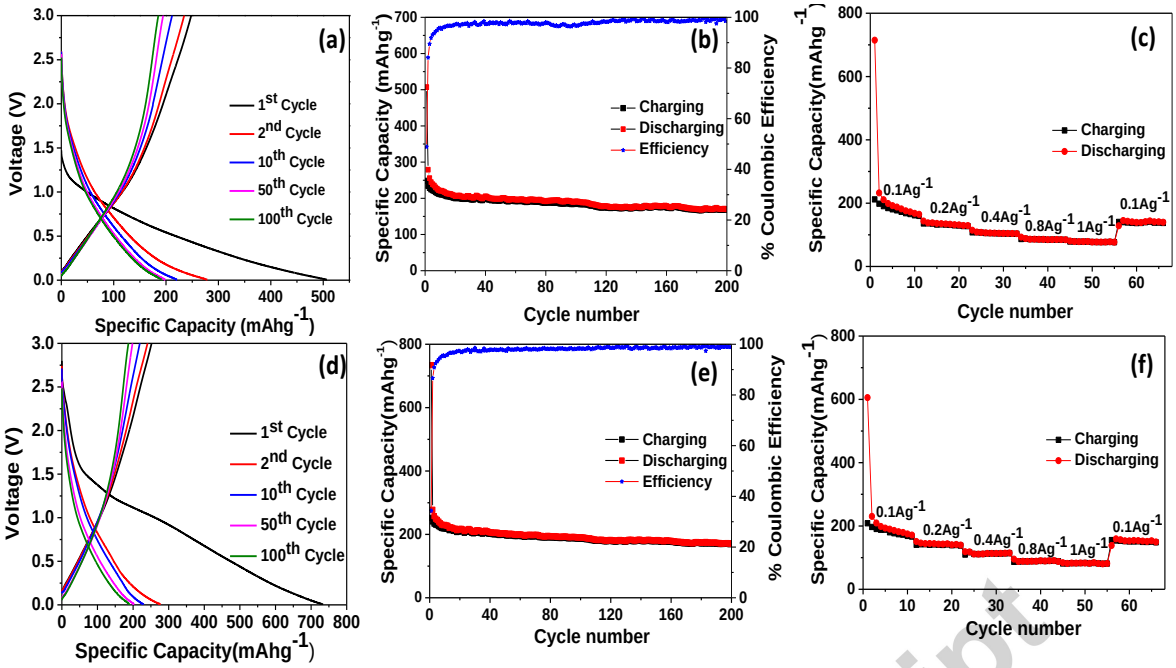

Fig. 3 Electrochemical performance of CNP and *c*-CNP tested against sodium: charge-discharge curves (a, d), cycling stability (b, e), and rate capability (c, f).

The rate performance of electrodes CNP and *c*-CNP was evaluated with current densities ranging from 100 to 1000 mAg^{-1}, and the results are shown in Fig. 3c and 3f. For sample CNP, specific capacities of 135, 107, 87 and 78 $mAhg^{-1}$ were obtained at current densities of 200, 400, 800, and 1000 mAg^{-1}, respectively. Similarly, electrode *c*-CNPs delivered discharge capacities of 140, 109, 87 and 82 $mAhg^{-1}$ at current densities of 200, 400, 800 and 1000 mAg^{-1}, respectively. At higher current densities, the capacity is mainly due to the diffusion of sodium ion in and out the solid electrode. Fig. S5 shows the Nyquist plots of the carbon electrodes. A straight line in the low frequency region along with a depressed semicircle in the high frequency region can be seen. The impedance spectra were modelled with equivalent circuits, which are depicted in Fig. S6, where R_e represents the resistance arising from contacts (sum of all the electrical resistances), C_{Lc} represents the double layer capacitance, R_c is the charge transfer resistance, Z_w is the Warburg element associated with

ion diffusion in carbon electrode [17]). The SEI formation at the electrode surface results in a resistance and a capacitance named as C_{SF} and R_{SF} [17], respectively. The numerical values obtained from modelling are represented in the Table S2. It can be noted that the charge-transfer resistance is higher in the case of electrode CNP. The overall resistance R_c+R_{SF} of *c*-CNP is much less as compared to CNP as observed from the impedance spectroscopy. However, with respect to performance both the batteries delivered similar capacitance indicating that the effect of carboxyl group is negligible. Overall both CNP and *c*-CNP perhaps because of the high density of the samples in turn delivers a high capacity.

Table 1 compares the performance of CNP and *c*-CNP vs Na/Na^+ with that of the literature. Carbons included in comparison are hard carbon particles [36], templated carbon [37], carbon fibers [38], graphene nanosheets [39], carbon nanotubes [39], nitrogen-doped carbon nanofibers [40], carbon microspheres [41], highly disordered carbon [13], banana peel derived pseudographite [17] and nanocellular carbon [42]. The performance of as prepared carbons is comparable with that of highly disordered carbons[13] whose discharge capacity is about 255 at 100 mAg^{-1}. The carbons reported in the present work has a highly reversible capacity, good cycling performance and high rate capability when tested against sodium, as compared to the previous reports.

Table 1. Comparison of electrochemical performance of carbon nanoparticles prepared in this work with other carbon electrode materials

Material	**Initial Coulombic Efficiency (%)**	**Discharge Capacity ($mAhg^{-1}$)(Cycle 2)**	**Reference**
CNP	49	278 at 100 mAg^{-1}	(this work)
c-CNP	34	277 at 100 mAg^{-1}	(this work)
Hard carbon particles	78	250 at 25 mAg^{-1}	[36]
Templated carbon	20	180 at 74 mAg^{-1}	[37]

Carbon fibers	46	ca. 350 at 50 mAg^{-1}	[38]
Graphene nanosheets	NA	220 at 30 mAg^{-1}	[39]
Carbon nanotubes	NA	82 at 30 mAg^{-1}	[39]
Nitrogen-doped carbon nanofibers	64	293 at 50 mAg^{-1}	[40]
Carbon microspheres	NA	202 at 30 mAg^{-1}	[41]
Highly disordered carbon	57.6	255 at 100 mAg^{-1}	[13]
Banana peel derived carbon	71	371 at 50 mAg^{-1}	[17]
Nanocellular carbon	NA	152 at 100 mAg^{-1}	[42]

3.2 Electrochemical performance as a lithium-ion battery anode

The obtained carbon materials were also evaluated as an anode for LIBs. The CV curves of CNP and *c*-CNP measured between 0.005 to 3 V with a sweep rate of 0.1 mVs^{-1} are shown in Fig. S7. The cathodic peak at around 0.76 V relates to the electrolyte decomposition on the surface of the electrode, leading to the formation of SEI [4]. The other peak at ~1.5 V corresponds to the reaction of lithium with some functional groups present on the carbon surface as observed previously [43]. A sharp reduction peak near 0 V can be attributed to the lithium intercalation with carbons representing sharp diffusion path of lithium ions [44]. After the first cycle, the CV curve overlap on each other indicating the reversibility of lithium storage in the electrodes.

The charge-discharge curves (Fig. 4a and 4d) show a slope from ~0 to 1.5 V, corresponding to the lithium deintercalation from the graphitic domains, and the slope above 1.5 V can be ascribed to extraction of lithium from defect sites with higher energies like vacancies as observed previously [43, 45]. Both CNP and *c*-CNP exhibited a high discharge capacity of 1330 and 1231 $mAhg^{-1}$ during the initial cycle, but with a poor coulombic

efficiency which was about 50 and 55% for CNP and *c*-CNP, respectively. It is reasonable to assume that the degree of irreversible trapping of lithium within the bulk of the carbon would affect the first cycle coulombic efficiency values, due to the formation of SEI on the surface of electrode [17]. Such capacity loss in the initial cycles is common amongst carbon materials.

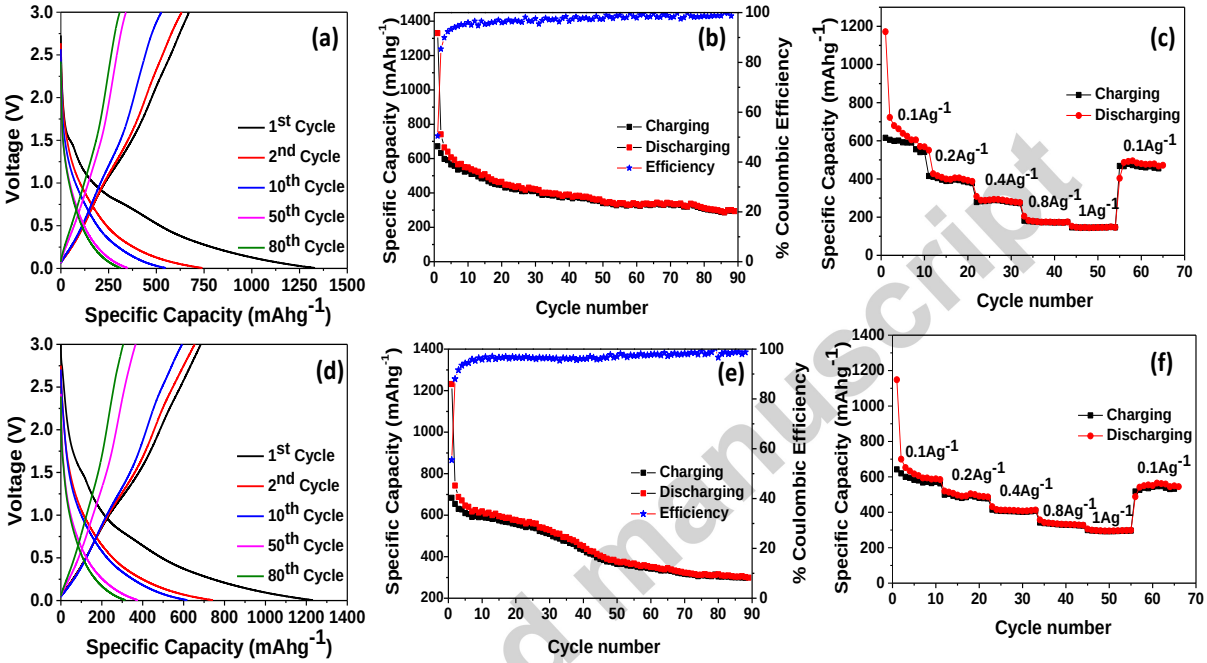

Fig. 4 Electrochemical performance of CNP and *c*-CNP tested against lithium: charge-discharge curves (a, d), cyclic stability (b, e), and rate capability (e, f).

The CNP and *c*-CNP showed reversible capacities of 741 and 742 $mAhg^{-1}$ respectively at the 2nd cycle and after 20 cycles the capacities became 464 and 577 $mAhg^{-1}$ respectively i.e., 37% and 22% capacity losses (Table S3). These results are in sharp contrast when compared to the performance of the as prepared carbon materials in NIBs, where no distinction in the cycling profile was observable. It was found that *c*-CNP exhibited a greater capacity than CNP in LIBs during cycling [21].

The effect of carboxyl group is more pronounced in the case of LIBs. It can be inferred from cyclic performance that, *c*-CNP has a higher capacity retention as compared to that of CNP (Fig. 4b and 4e). This is credited to the presence of carboxyl group that can provide a reversible lithium interaction [21]. This may be due to the formation of organic lithium salts with carboxyl groups ($-COO^- Li^+$) present on *c*-CNP which serve as a passive layer causing the reduction of irreversible capacity to a minimum value [20]. A noticeable difference is that, the capacity of the carbon samples as an anode for LIBs is thrice that for NIBs. The carboxyl group has a substantial effect while testing against lithium unlike sodium where the effect is negligible. This may be due to the larger size of sodium ion which might show lesser affinity to form such organic salts with carboxyl groups.

The rate capability of CNP and *c*-CNP vs Li is shown in the Figs. 4c, 4f. For sample CNP, specific capacities of 427, 309, 183 and 149 $mAhg^{-1}$ were observed at current densities of 200, 400, 800 and 1000 mAg^{-1}, respectively. For sample *c*-CNP, a capacity of 499, 409, 336 and 295 $mAhg^{-1}$ were obtained at current densities of 200, 400, 800 and 1000 mAg^{-1}. The higher rate capability and better reversibility can be seen from electrode *c*-CNP when compared to CNP which is again credited to the presence of carboxyl groups. The Nyquist plots for both CNP and *c*-CNP electrodes (Fig. S9) displayed a depressed semi-circle spiked at the lower frequency region, similar to that of NIB. From the semicircle, $R_{SF}+R_C$ value can be obtained and are listed in Table S3 [46]. It can be observed that the $R_{SF}+R_C$ is lower in case of *c*-CNP as compared with CNP, showing that the former has a faster charge transfer kinetics than the latter. A comparison with the state of art carbon is represented Table 2. Carbons included for comparison are graphene [47], graphene nanosheets [48], banana peel derived carbon [17], nitrogen rich porous carbon spheres [49], graphene/carbon nanofibers [50], nitrogen-doped Graphitic carbon spheres [51], graphitic carbon spheres [51], porous carbon nanofibers [52], carbon nanofibers [53] and carbon nanospheres [54]. From the Table

2 it can be evaluated that the overall performance of the carbons prepared in this work is excellent in terms of cycling and capacity retention, only slightly inferior to that of the banana-peel-derived carbon [17].

Table 2. Comparison of CNP & *c*-CNP with the state of art LIBs

Material	Initial Coulombic Efficiency (%)	Discharge Capacity ($mAhg^{-1}$) (2^{nd} cycle)	Reference
CNP	50	741 at 100 mAg^{-1}	**(this work)**
***c*-CNP**	55	742 at 100 mAg^{-1}	**(this work)**
Graphene	38	580 at 25 mAg^{-1}	**[47]**
Graphene nanosheets	NA	784 at 50 mAg^{-1}	**[48]**
Banana peel derived carbon	69	826 at 50 mAg^{-1}	**[17]**
Nitrogen rich porous carbon spheres	64	631 at 0.5 Ag^{-1}	**[49]**
Graphene/carbon nanofibers	55	667 at 0.12 $mAcm^{-2}$	**[50]**
Nitrogen doped Graphitic carbon spheres	49	840 at 50 mAg^{-1}	**[51]**
Graphitic carbon spheres	NA	ca. 550 at 50 mAg^{-1}	**[51]**
Porous carbon nanofibers	66	ca. 491 at 50 mAg^{-1}	**[52]**
Carbon nanofibers	NA	483 at 50 mAg^{-1}	**[53]**
Carbon nanospheres	72	ca. 800 at 50 mAg^{-1}	**[54]**

4. Conclusion

Carbon nanoparticles prepared from coconut oil using the flame deposition method showed good performance as anode in both sodium-ion and lithium-ion batteries. The carbon electrode exhibited a second-cycle discharge capacity of about 277 $mAhg^{-1}$ in a sodium-ion battery and of about 741 $mAhg^{-1}$ in a lithium-ion battery at a current density of 100 mAg^{-1}.

The stability of the carbon nanoparticles against cycling can be significantly improved by surface modification. Electrode was found to be highly stable in terms of charge-storage and efficiency. The effect of surface chemistry of the carbon nanoparticles on electrochemical performance was found to be distinctly observable in the case of lithium-ion batteries. However, no such effect was found in the case of NIBs. Hence, different chemistries seem to be present for the interactions between carbon nanoparticles before and after treatment in lithium and sodium ion battery systems. Further investigation on the interaction of sodium ions with carboxyl groups will be carried out in future. This research showed that biomass-derived carbon nanoparticles are potential anode materials for high performance batteries.

Acknowledgements

This research was supported by the Australian Research Council (Projects FT100100879 and DP130101870). RRG acknowledges the scholarships granted by The University of Queensland. NAK thanks the University of Queensland for UQ fellowship. The authors gratefully acknowledge the facilities, scientific and technical assistance of the Australian Microscopy and Microanalysis Research Facility at the UQ Centre for Microscopy and Microanalysis.

Appendix A. Supplementary material

Supplementary data associated with this article can be found in the online version at http://dx.doi.org/xxx.

References

[1] E. Peled, C. Menachem, D. Bar-Tow, A. Melman, J. of the Electrochem. Soc., 143 (1996) L4-L7.

[2] Y. Cao, L. Xiao, X. Ai, H. Yang, Electrochem. and solid-state lett., 6 (2003) A30-A33.

[3] Y. Kim, K.H. Ha, S.M. Oh, K.T. Lee, Chem.- Eur. J., 20 (2014) 11980-11992.

[4] D. Stevens, J. Dahn, J. of the Electrochem. Soc., 148 (2001) A803-A811.

[5] L. Wu, D. Buchholz, D. Bresser, L. Gomes Chagas, S. Passerini, J. of Power Sources, 251 (2014) 379-385.

[6] R. Alcántara, M. Jaraba, P. Lavela, J.L. Tirado, Chem. of Mater., 14 (2002) 2847-2848.

[7] H. Xiong, M.D. Slater, M. Balasubramanian, C.S. Johnson, T. Rajh, J. of Phys. Chem. Lett., 2 (2011) 2560-2565.

[8] Y. Xu, E. Memarzadeh Lotfabad, H. Wang, B. Farbod, Z. Xu, A. Kohandehghan, D. Mitlin, Chem. Comm., 49 (2013) 8973-8975.

[9] K.-T. Kim, G. Ali, K.Y. Chung, C.S. Yoon, H. Yashiro, Y.-K. Sun, J. Lu, K. Amine, S.-T. Myung, Nano Lett., 14 (2014) 416-422.

[10] L. David, R. Bhandavat, G. Singh, ACS Nano, 8 (2014) 1759-1770.

[11] X. Li, M.M. Hasan, A.L. Hector, J.R. Owen, J. of Mater. Chem. A, 1 (2013) 6441-6445.

[12] Q. Fan, W. Zhang, J. Duan, K. Hong, L. Xue, Y. Huang, Electrochim. Acta, 174 (2015) 970-977.

[13] X. Zhou, Y.G. Guo, ChemElectroChem, 1 (2014) 83-86.

[14] E. Irisarri, A. Ponrouch, M. Palacin, J. of the Electrochem. Soc., 162 (2015) A2476-A2482.

[15] H. Hou, C.E. Banks, M. Jing, Y. Zhang, X. Ji, Adv. Mater., 27 (2015) 7861-7866.

[16] Y. Bai, Z. Wang, C. Wu, R. Xu, F. Wu, Y. Liu, H. Li, Y. Li, J. Lu, K. Amine, ACS Appl. Mater. Interfaces, 7 (2015) 5598-5604.

[17] E.M. Lotfabad, J. Ding, K. Cui, A. Kohandehghan, W.P. Kalisvaart, M. Hazelton, D. Mitlin, ACS Nano, 8 (2014) 7115-7129.

[18] P. Kalyani, A. Anitha, Int. J. of Hydrogen Energy, 38 (2013) 4034-4045.

[19] Y. Yao, F. Wu, Nano Energy, 17 (2015) 91-103.

[20] Y. Ein-Eli, V.R. Koch, J. of the Electrochem. Soc., 144 (1997) 2968-2973.

[21] Z. Xie, Z. Yu, W. Fan, G. Peng, M. Qu, RSC Adv., 5 (2015) 90041-90048.

[22] R.R. Gaddam, D. Vasudevan, R. Narayan, K.V.S.N. Raju, RSC Adv., 4 (2014) 57137-57143.

[23] R.R. Gaddam, S. Kantheti, R. Narayan, K.V.S.N. Raju, RSC Adv., 4 (2014) 23043-23049.

[24] D.S. Knight, W.B. White, J.of Mater. Res., 4 (1989) 385-393.

[25] N.A. Kumar, H.-J. Choi, Y.R. Shin, D.W. Chang, L. Dai, J.-B. Baek, ACS Nano, 6 (2012) 1715-1723.

[26] K.J. Ziegler, Z. Gu, H. Peng, E.L. Flor, R.H. Hauge, R.E. Smalley, J. American Chem. Soc., 127 (2005) 1541-1547.

[27] G.X. Chen, M.H. Hong, T.C. Chong, H.I. Elim, G.H. Ma, W. Ji, J. of Appl. Phys., 95 (2004) 1455-1459.

[28] J. Chen, M.A. Hamon, H. Hu, Y. Chen, A.M. Rao, P.C. Eklund, R.C. Haddon, Science, 282 (1998) 95-98.

[29] K.S. Sing, J. Rouquerol, Adsorption at the gas-solid and liquid-solid interface, Elsevier2009.

[30] G. Xu, J. Han, B. Ding, P. Nie, J. Pan, H. Dou, H. Li, X. Zhang, Green Chem., 17 (2015) 1668-1674.

[31] K. Nanjundan Ashok, B. Jong-Beom, Nanotechnology, 26 (2015) 492001.

[32] S. Kajiyama, L. Szabova, K. Sodeyama, H. Iinuma, R. Morita, K. Gotoh, Y. Tateyama, M. Okubo, A. Yamada, ACS Nano, (2016).

[33] Y. Cao, L. Xiao, M.L. Sushko, W. Wang, B. Schwenzer, J. Xiao, Z. Nie, L.V. Saraf, Z. Yang, J. Liu, Nano Lett., 12 (2012) 3783-3787.

[34] H. Wang, W. Yu, J. Shi, N. Mao, S. Chen, W. Liu, Electrochim. Acta, 188 (2016) 103-110.

[35] T. Yang, T. Qian, M. Wang, X. Shen, N. Xu, Z. Sun, C. Yan, Adv. Mater., 28 (2016) 539-545.

[36] S. Komaba, W. Murata, T. Ishikawa, N. Yabuuchi, T. Ozeki, T. Nakayama, A. Ogata, K. Gotoh, K. Fujiwara, Adv. Funct. Mater., 21 (2011) 3859-3867.

[37] S. Wenzel, T. Hara, J. Janek, P. Adelhelm, Energy & Environ. Sci., 4 (2011) 3342-3345.

[38] L. Fu, K. Tang, K. Song, P.A. van Aken, Y. Yu, J. Maier, Nanoscale, 6 (2014) 1384-1389.

[39] X.-F. Luo, C.-H. Yang, Y.-Y. Peng, N.-W. Pu, M.-D. Ger, C.-T. Hsieh, J.-K. Chang, J. Mater. Chem. A, 3 (2015) 10320-10326.

[40] J. Zhu, C. Chen, Y. Lu, Y. Ge, H. Jiang, K. Fu, X. Zhang, Carbon, 94 (2015) 189-195.

[41] T. Chen, L. Pan, T. Lu, C. Fu, D.H.C. Chua, Z. Sun, J. Mater. Chem. A, 2 (2014) 1263-1267.

[42] Y. Shao, J. Xiao, W. Wang, M. Engelhard, X. Chen, Z. Nie, M. Gu, L.V. Saraf, G. Exarhos, J.-G. Zhang, J. Liu, Nano Lett., 13 (2013) 3909-3914.

[43] K. Tang, R.J. White, X. Mu, M.M. Titirici, P.A. van Aken, J. Maier, ChemSusChem, 5 (2012) 400-403.

[44] M. Kakunuri, C.S. Sharma, Electrochim. Acta, 180 (2015) 353-359.

[45] N.A. Kaskhedikar, J. Maier, Adv. Mater., 21 (2009) 2664-2680.

[46] P. Kollu, P.R. Kumar, C. Santosh, D.K. Kim, A.N. Grace, RSC Adv., 5 (2015) 63304-63310.

[47] A. Kumar, A.L.M. Reddy, A. Mukherjee, M. Dubey, X. Zhan, N. Singh, L. Ci, W.E. Billups, J. Nagurny, G. Mital, P.M. Ajayan, ACS Nano, 5 (2011) 4345-4349.

[48] E. Yoo, J. Kim, E. Hosono, H.-s. Zhou, T. Kudo, I. Honma, Nano Lett., 8 (2008) 2277-2282.

[49] D. Li, L.-X. Ding, H. Chen, S. Wang, Z. Li, M. Zhu, H. Wang, J. Mater. Chem. A, 2 (2014) 16617-16622.

[50] Z.-J. Fan, J. Yan, T. Wei, G.-Q. Ning, L.-J. Zhi, J.-C. Liu, D.-X. Cao, G.-L. Wang, F. Wei, ACS Nano, 5 (2011) 2787-2794.

[51] S.-X. Wang, S. Chen, Q. Wei, X. Zhang, S.Y. Wong, S. Sun, X. Li, Chem. Mater., 27 (2015) 336-342.

[52] J. Liwen, Z. Xiangwu, Nanotechnology, 20 (2009) 155705.

[53] L. Ji, X. Zhang, Electrochem. Commun., 11 (2009) 684-687.

[54] Y. Chen, Z. Lu, L. Zhou, Y.-W. Mai, H. Huang, Nanoscale, 4 (2012) 6800-6805.

Mr. Rohit Ranganathan Gaddam is a PhD student at The University of Queensland under the supervision of Prof. X.S. Zhao and Dr. Ashok Kumar Nanjundan. He has been awarded with IPRS and UQ Centennial Scholarships for his PhD study. He has previously worked at CSIR-Indian Institute of Chemical Technology as a researcher. He has also carried out research work at CSIR-Central Glass & Ceramic Research Institute and CSIR-Central Electrochemical Research Institute in India. He holds an M.Tech degree in nanotechnology. His research interests are focused on bio-derived carbon materials for energy storage devices.

Ms. Dongfang Yang received her both BS and MS in Material Science and Engineering from Central South University (China) in 2011 and 2014, respectively. She is now a PhD student in the School of Chemical Engineering at The University of Queensland (Australia) under the supervision of Prof. X.S. Zhao and Dr Ashok Kumar Nanjundan. Her PhD project is regarding anode materials for sodium-ion energy storage devices.

Dr. KVSN Raju is an Advisor of Polymers and Functional Materials Division, CSIR-Indian Institute of Chemical Technology, Hyderabad, India. He received his Masters and Ph.D. degrees in chemistry from Osmania University, Hyderabad, India and then worked with Prof. Werner Funke's at the Max Plank Institute, Germany during 1987–89 under the DAAD Exchange program. His research focused on organic–inorganic hybrids, functionalization of nanomaterials and polymers, hyperbranched polymers, thermoset polymers and use of triazoles chemistry for the development of functional polymers etc.

Dr. Ramanuj Narayan is a Principal Scientist at Polymers & Functional Materials Division of CSIR-IICT. He completed his M. Tech (1996) from at National Institute of Technology, Jamshedpur. His PhD (2002) work focused on the development of high solids & water dispersible coatings at CSIR-IICT under the supervision of Dr KVSN Raju. Prior to joining IICT, he worked as Research Scientist at Asian Cosmos R&D Co. Ltd. (2002), Research division at Tata Steel Ltd (2006) and as a Senior Scientist at Tata AutoComp Systems Limited (2007). His research focuses on nanomaterials, third generation solar cell, organic, polymeric & hybrid materials for functional coatings and composites.

Dr. Ashok Kumar Nanjundan is a UQ Postdoctoral Fellow at The University of Queensland. After spending 3 years at TU Dresden he moved to South Korea where he received his PhD from Pukyong National University in 2010. He then joined the Ulsan National Institute of Science and Technology as a postdoctoral fellow. In 2011 he was awarded the Marie-Curie fellowship *Eurotalents* at the French Atomic Energy Commission. He later moved to Trinity College Dublin as a research fellow. In 2012, he was awarded the JSPS postdoctoral fellowship at Kumamoto University. Ashok's research focuses on the synthesis of carbon based nanostructured materials and polymers, in particular, the implementation of such materials in emerging energy applications.

Dr. George Zhao is a professor at the School of Chemical Engineering, The University of Queensland (UQ) where he completed his PhD study in 1999. He is the director of Clean Energy and Water Research program at UQ. Prior to joining UQ in 2011, he was an Associate Professor at the National University of Singapore. Dr. Zhao is a fellow of the Royal Society of Chemistry. He serves a couple of scientific journals as an editorial board member or international advisory board member. Professor Zhao's current research interest is on porous materials for energy and water applications.

Highlights

- Carbon nanoparticles were prepared from biomass
- The carbon nanoparticles were shown to be a robust anode material with high discharge capacities for both sodium-ion batteries and lithium-ion batteries.
- The carbon nanoparticles exhibited superior rate and cycling performance for both sodium-ion batteries and lithium-ion batteries.